Results and analysis of free-electron-laser oscillation in a high-energy storage ring

M. E. Couprie
Commissariat à l'Energie Atomique, Département des Sciences de la Matière, Service de Physique des Atomes et des Surfaces, Centre d'Etudes Nucléaires de Saclay, 91191 Gif-sur-Yvette, France and Laboratoire d'Utilisation du Rayonnement Electromagnétique, Centre National de la Recherche Scientifique, Commissariat à l'Energie Atomique, Ministère de l'Education Nationale, de la Jeunesse et des Sports Bâtiment 209 D, Université de Paris–Sud, 91405 Orsay CEDEX, France

M. Velghe
Laboratoire de Photo-Physique Moléculaire, Bâtiment 213, Université de Paris–Sud, 91405 Orsay CEDEX, France and Laboratoire d'Utilisation du Rayonnement Electromagnétique, Centre National de la Recherche Scientifique, Commissariat à l'Energie Atomique, Ministère de l'Education Nationale, de la Jeunesse et des Sports, Bâtiment 209 D, Université de Paris–Sud, 91405 Orsay CEDEX, France

R. Prazeres and D. Jaroszynski
Commissariat à l'Energie Atomique, Département des Sciences de la Matière, Service de Physique des Atomes et des Surfaces, Centre d'Etudes Nucléaires de Saclay, 91191 Gif-sur-Yvette, France and Laboratoire d'Utilisation du Rayonnement Electromagnétique, Centre National de la Recherche Scientifique, Commissariat à l'Energie Atomique, Ministère de l'Education Nationale, de la Jeunesse et des Sports, Bâtiment 209 D, Université de Paris–Sud, 91405 Orsay CEDEX, France

M. Billardon
Ecole Supérieure de Physique et Chimie Industrielles, 10 rue Vauquelin, 75231 Paris CEDEX, France and Laboratoire d'Utilisation du Rayonnement Electromagnétique, Centre National de la Recherche Scientifique, Commissariat à l'Energie Atomique, Ministère de l'Education Nationale, de la Jeunesse et des Sports, Bâtiment 209 D, Université de Paris–Sud, 91405 Orsay CEDEX, France

(Received 20 December 1990)

A storage-ring free-electron laser at Orsay has been operating since 1989 in the visible wavelength range. In contrast with previous experiments, it operates with positrons and at higher energies (600–800 MeV), with the storage ring Super-ACO (ACO denotes Anneau de Collisions d'Orsay). The optical gain, the laser power, the transverse profile, and the macrotemporal structure of the laser are analyzed. In particular, we show that the gain matrix possesses many off-diagonal elements, which results in lasing on a combination of noncylindrical Gaussian modes. The eigenmode of the laser oscillation is a combination of one or two main Gaussian modes and several higher-order modes, which results in most of the power being extracted in these modes.

I. INTRODUCTION

The first storage-ring free-electron laser (SRFEL) was operated in 1983 using the old storage ring, ACO (Anneau de Collisions d'Orsay), at Orsay, France [1]. Despite the nonoptimal performance of the storage ring, constructed in 1965, studies were conducted over several years, yielding valuable experimental data on FEL physics and, moreover, demonstrating the feasibility of such a laser in the visible and uv wavelength range. The second SRFEL to operate was in 1988 at Novosibirsk VEPP3 [2] (VEPP3 stands for electron and positron beams in collision, in Russian) initially in the visible wavelength range and then later in the uv. A third SRFEL operated in 1989 using the storage ring Super-ACO at Orsay [3,4]. In the latter experiment the major difference, compared with the previous experiments, was a higher positron energy (600–800 MeV), larger than both ACO (200 MeV) and VEPP3 (350 MeV). The higher energy has led to an enhancement of the laser power, and the better performances of the storage ring have also improved the optical gain. However, this is partially counterbalanced by a reduction in gain due to the higher energy as the gain evolves as E^{-3}. The resultant net gain was therefore around 2% per pass. In this paper we describe the main results obtained on the Super-ACO SRFEL. In general, the behavior of the laser differs from the behavior observed in previous experiments, for the laser power, the macrotemporal structure, the transverse profile of the optical field, the irradiation of mirrors with a high level of short wavelengths, and a particular sensitivity to the coherent synchrotron oscillations.

II. GENERAL DESCRIPTION OF THE SUPER-ACO FEL EXPERIMENT

A storage-ring free-electron-laser experiment can be described as the combination of three distinct elements:

the storage ring, which provides the electron or positron beam; the undulator or optical klystron, which can be considered as the amplifying medium; and the optical cavity, which stores the optical radiation leading to the laser oscillation. Detailed descriptions of these elements are to be found in the general FEL literature. In this section we only give a brief description of these elements for the case of the Super-ACO. Particular aspects of the interaction between the elements will be given in a subsequent section devoted to the description of the FEL itself.

A. Super-ACO storage ring

The Super-ACO storage ring has operated since March 1987 at Laboratoire pour l'Utilisation du Rayonnement Electromagnétique at Orsay [5]. Table I lists the main parameters. The 0.8-GeV machine is injected with positrons, to provide a good stability and lifetime. The Super-ACO is mainly devoted to synchrotron radiation and belongs to the new generation of machines that includes various magnetic insertion devices. However, for FEL operation, the particular experimental conditions detailed later in Sec. III exclude, at least for the moment, concurrent use of the storage ring for classical synchrotron-radiation experiments.

B. Optical klystron

For a FEL on the storage ring, a simple undulator gives a low optical gain. As in previous experiments on the ACO [1] and the VEPP3 [2], an optical klystron is chosen to enhance the optical gain by a factor of 5. The construction and optimization of this optical klystron were described in a previous paper [6], and the main parameters are listed in Table II.

The choice of a 13-cm undulator period length gives a maximum K value of 5.75, and therefore the spectral range available on the first harmonic with the undulator extends from 1.8 to 0.13 μm, attainable by modifying both the K value and the beam energy (between 400 and 800 MeV).

TABLE I. Characteristics of the Super-ACO at 800 MeV.

Number of bunches	1–24
Current per bunch	100 mA
Energy spread	5.3×10^{-4}
Emittance	
Horizontal	4×10^{-8} m rad
Vertical	2×10^{-9} m rad
Beam sizes	
Length	90 ps
Horizontal (vertical)	225 μm (125 μm)
Threshold of anomalous bunch lengthening	7 mA
Energy range	550–800 MeV
rf	
Frequency	100 MHz
Voltage	150 MHz

The choice of the dispersive section (strength and length) is related to the gain and power optimization. The performance of the dispersive section is determined by the phase shift α between the light emitted in the first undulator and that emitted in the second undulator, and is defined by the interference order between the two undulators $N+N_d=2\pi\alpha$ [13]. N represents the number of periods of one undulator, and N_d is the effective number of periods (or fraction of periods) dependent on the strength of the dispersive section; N_d also depends on the wavelength and the electron energy as $(1/\lambda\gamma^2)$. For optimum gain $N+N_d=(4\pi\sigma_\gamma/\gamma)^{-1}$, where σ_γ/γ is the energy spread without the laser on. The optimization of the power is also given by this relation, where σ_γ/γ is now the energy spread with laser on [6]. Then the optimization of gain or power requires a large adjustment of N_d (that is to say, of the magnet gap) following the experimental conditions for the wavelength, the electron energy, and the energy spread.

For the Super-ACO the minimum energy spread is of the order of $\sigma_\gamma/\gamma\simeq5\times10^{-4}$; therefore the optimum operation a value of $N+N_d=150$ is required. The dispersive section has been chosen to realize a maximum value of $N+N_d=100$ for $\lambda=0.6$ μm and $E=800$ MeV, to enable the optimzation to be performed only by adjusting the magnet gap over the range of magnetic field from 0 to 0.5 T, independent of the electron energy and the energy spread, for all wavelengths in the uv, visible, and near-infrared spectrum.

The predicted gain for the optical klystron is approximately 1% (see Table 4 of Ref. [6]). Experimental measurements detailed in Sec. III yielded somewhat higher values than this.

An important requirement for the insertion device is the absence of perturbations of the stored electron beam resulting from the systematic vertical focusing (no modification of the orbit and no additional tune shift).

TABLE II. Characteristics of the optical klystron.

Total length L_{OK}	3.1m
Magnet characteristics	
Dimensions	$32\times32\times50$ mm^3
Material	$SmCo_5$
Manufacturer	UGIMAG (France); type, Recoma 22
Remnent field	0.9 T
Undulator characteristics	
Period	12.9 cm
Number of periods	10
Total length (1 undulator)	1.3 m
Number of magnets layers	1
Number of magnets per period	16
On-axis magnetic field	0–0.48 T
Dispersive section characteristics	
Length	0.5 m
Number of magnets layers	2
On-axis magnetic field	0–0.5 T
Vacuum chamber	
Inside gap	30 mm
Outside gap	38 mm

C. Optical cavity

1. Optimization

The optimization of the optical cavity relies on the longitudinal and transverse overlap between the positron bunch and the light pulse. The longitudinal overlap requires that the distance between two bunches should match the cavity length exactly for synchronization. This condition maximizes the amplification on each pass. The presence of the physical constraints of concrete walls led to a choice of an 18-meter-long optical cavity, for two-positron-bunch operation. The optical klystron is slightly off center by 1 m with respect to the center of the optical cavity. The choice of confocal parameters of the cavity depends on the transverse size of the positron beam in the cavity. The gain reduction is taken into account with a "filling factor." For a TEM_{00} laser mode, this can be expressed as [7]

$$F_f=\left\{\left[1+\left[\frac{w_0}{2\sigma_x}\right]^2\right]\left[1+\left[\frac{w_0}{2\sigma_z}\right]^2\right]\right\}^{1/2} f_c(w_0,\sigma_x,\sigma_z)\ . \tag{1}$$

The correction factor f_c gives the effect of the dynamic change of the positron position relative to the laser beam waist w_0, and depends on the dimensionless parameters Σ characterizing the transverse dimensions of the positron beam and W the laser beam waist. The first term of Eq. (1) is optimized for a circular-cross-section particle beam, with identical transverse dimensions, i.e., σ. A factor of 2 between the two sizes σ_x,σ_y reduces the gain by roughly 5%. For a circular-section beam, one has

$$\Sigma=\sigma\sqrt{\pi/\lambda L_{OK}},\quad W=w_0\sqrt{\pi/\lambda L_{OK}}\ ,$$

where L_{OK} is the optical klystron length. The ratio of those two magnitudes is therefore the ratio of the transverse size over the laser beam waist. W depends only on the geometry of the optical cavity, and for a symmetrical cavity of length d and mirror curvature R_c is given by

$$W=[\sqrt{d(2R_c-d)}/2L_{OK}]^{1/2}\ .$$

The optimum W is around 0.45 for an optical klystron, though the range is rather large. One has, however, to avoid $W=0$, the stability limit of the optical cavity. Figure 1 shows how the multiplicative factor F_f depends on W and Σ. If the electronic density is not constant, the optimization presented above must be performed on $\rho_e F_f$.

On the Super-ACO, Σ ranges between 0.1 and 1, following the experimental conditions leading to an optimum value for W close to $W=0.9$. The 10-m radius of curvature for the mirror is chosen because of fabrication standards. Nevertheless it does correspond to a limit case for the optimization of the cavity. Apart from the infrared, diffraction losses are negligible for a TEM_{00} mode because the Frensel number $N=r^2/\lambda d$ is larger than 2 (r is the radius of the mirrors). The characteristics of the Super-ACO optical cavity are shown in Table III.

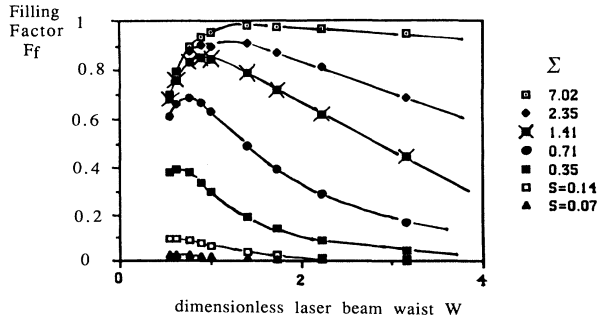

FIG. 1. Filling factor for a TEM_{00} mode vs the Σ and W parameters.

2. Mirror degradation

The rather low value of the gain does not allow the use of metallic mirrors; multidielectric-layer mirrors must be used in spite of their bandwidth being rather smaller. The mirrors installed in the optical cavity are continually submitted to strong radiation from the undulators of the optical klystron. The spectral distribution extends towards the higher harmonics when the storage-ring energy and the deflection parameters are larger (Fig. 2). The effects of this irradiation, largely studied at Orsay, are detailed in Refs. [8] and [9].

Roughly, the undulator emission can be characterized by two parameters: the total emitted power and the critical wavelength. Their dependence versus the ring energy, the current, and the deflection parameter K as the following dependence:

$$P\propto E^2K^2I,\quad \lambda_c\propto 1/(E^2K)\ . \tag{2}$$

Table IV shows examples of the total emitted power for 100 mA in the ring and the critical wavelength on the Super-ACO.

Tests on the Super-ACO have been performed on the storage ring at 800 MeV with $K=5$ and mirrors manufactured by Balzers. The measured losses reached 0.1% at 633 nm, after irradiation. The mirrors were measured before insertion in the vacuum chamber, then irradiated, and finally removed and remeasured. This procedure cannot measure a quick reversibility or recovery in the air. The measurement only gives an order of magnitude of the losses. However, when they are significantly smaller than the gain value (by a factor of 2, for instance), FEL operation is reasonably easily obtained.

TABLE III. Characteristics of the Super-ACO optical cavity.

Mirror distance d	18 m	Divider of cT_0
Mirror curvature R_c	10 m	$R_c=(4L_{OK}^2W^4+d^2)/2d$
W	1	
Rayleigh length Z_0	3.1 m	$Z_0=W^2L_{OK}$
w_0	0.79 mm	At 630 nm; $w_0^2=Z_0/\pi$
w (middle undulator)	0.82 mm	At 630 nm
w (mirrors)	2.4 mm	At 630 nm

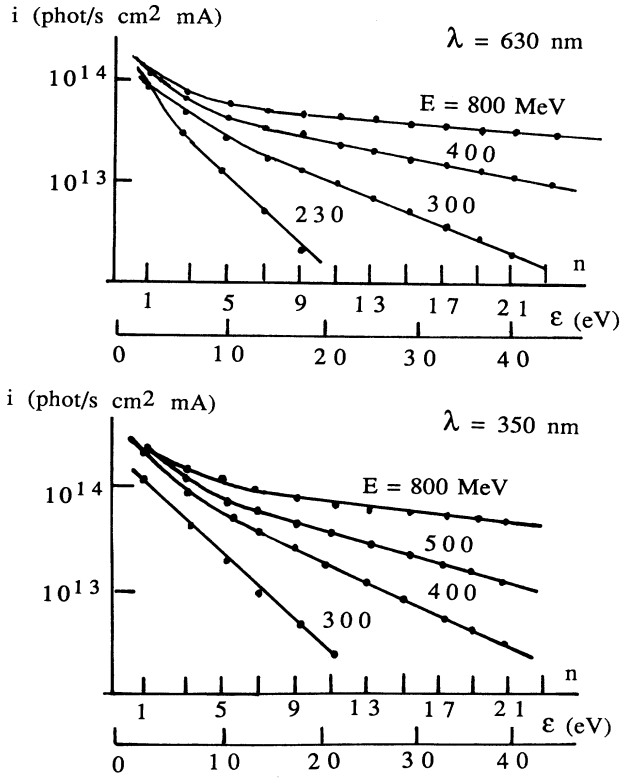

FIG. 2. Spectral distribution of the Super-ACO spontaneous emission for the fundamental wavelengths 6300 and 3500 Å, and for different electron energies values. Horizontal scales, harmonic number n and corresponding photon energy ε (eV). Vertical scale, flux of photons per cm^2 and mA.

III. OPERATING POINT OF SUPER-ACO

The FEL performances depend on several parameters. Some, such as the undulator characteristics, are fixed by the initial choice when designing the optical klystron. Some others can be adjusted, such as the energy or the magnetic transport optics of the ring. After these initial choices have been made the FEL performance depends only on a limited number of parameters, i.e., energy spread, and longitudinal and transverse sizes of the electron bunch, all of which evolve with the ring current. In this section, we present some details on the main parameters that determine the optical gain.

A. Choice of the energy

The positron beam energy can be set between 800 MeV, the nominal energy, the low emittance optics of the ring being used, and 400 MeV, in principle, if the "high-emittance" optics is used. Using a high energy, such as 800 MeV, results in mirror degradation, induced by the intense and large bandwidth emission from the undulators. In addition to thermal heating leading to geometric modification, there is also a possible destruction of the dielectric layers. This should, however, be compensated for at the higher energies by an enhancement of laser power. For lower energies, there is less degradation and a higher gain. However, the beam lifetime is reduced.

Nevertheless, the desired spectral range depends on the parameters of the undulator, such as K (varying up to 5.75) and the period (of 13 cm), and sets an upper bound for the energy. For example, the first operation of the FEL on the Super-ACO was centered at 633 nm, because of the mirror technology. This wavelength set an upper limit of 650 MeV for the energy. 600-MeV energy was finally selected. Let us note that this is still very high, when compared with the usual beam energies for FEL operation. The two preceding successful FEL experiments on storage rings employed a 240-MeV electron beam on the ACO [1,10,11] and a 350-MeV beam on the VEPP3 at Novosibirsk [2,12], and FEL's on linear and electrostatic accelerators usually operate with energies lower than 100 MeV.

TABLE IV. Total emitted power from the optical klystron of Super-ACO, for 100 mA of stored beam. The critical wavelength, characterizing the spectral repartition, is also given.

E (MeV)	K	P(100 mA) (W)	λ_c (Å)
800	5.75	25	60
600	5	9.5	120
400	3	2	460

B. Energy spread deduced from the spontaneous emission spectra of the optical klystron

The experimental spectrum of the optical klystron showing the effect of the interference of the two undulators is shown in Fig. 3. The analysis of such a spectrum gives the resonant wavelength λ_R, the undulator rate $f=(I_{\max}-I_{\min})/(I_{\max}+I_{\min})$, i.e., the contrast of fringes, the $(N+N_d)$ value from the fringe width, and the N value from the envelope shape. For the FEL, the most interesting parameters are $N+N_d$ and f, which permit the determination of the energy spread and therefore the possible gain. The best method is the simultaneous measurement of $N+N_d$ and f, over a large range of dispersive section gaps, and therefore leads to large variations of $(N+N_d)$. From the theoretical dependence of f versus $N+N_d$ [13],

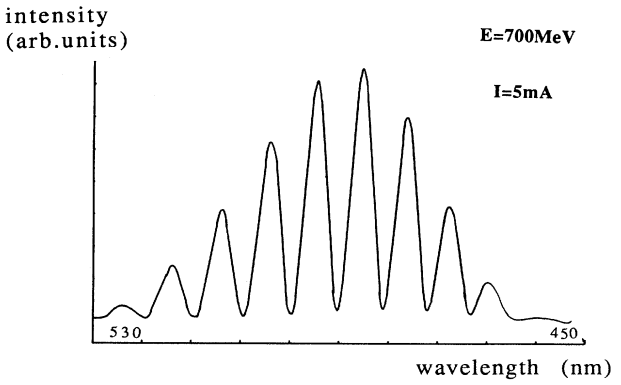

FIG. 3. An example of the spontaneous emission of the Super-ACO optical klystron. Energy, 700 MeV; resonant wavelength, 495 nm; dispersive section gap, 80 nm ($N+N_d=100$).

$$f = f_r \exp\{-\tfrac{1}{2}[4\pi(N+N_d)\sigma_\gamma/\gamma]^2\} , \quad (3)$$

one can deduce the energy spread σ_γ/γ and the residual modulation rate f_r due to other causes. The measured f_r value, $f_r = 0.989$, leads to a negligible gain reduction. Figure 4 shows the behavior of the energy spread versus the current at 600 MeV that is recorded for three different injections of beam in the Super-ACO. The behavior of the energy spread versus the storage-ring current is determined by the anomalous bunch lengthening. The bunch lengthening threshold is in the region of 6 mA per bunch. For higher currents, coherent or incoherent modes of bunch oscillations due to the interaction with the vacuum chamber enhance the bunch length and the energy spread by a factor of 2.

C. Bunch length

The bunch length is recorded on the Super-ACO by sampling the signal from a pickup station measuring the current field of the electron bunch directly on a fast oscilloscope. Difficulties arising from the response of the electrode and that of the detection system result in a signal that is generally related to the derivatives of the longitudinal distribution of the positron bunch.

An alternative indirect method is to deduce σ_γ from the energy spread, using the relationship

$$\sigma_1 = (\alpha/2\pi f_s)(\sigma_\gamma/\gamma) . \quad (4)$$

The momentum compression factor α, linked to the circumference dilation due to an energy change, has been determined by the spontaneous-emission spectra and the emission-fringes displacement, while changing the rf frequency, and is found to be equal to 1.4×10^{-2}. The synchrotron frequency is measured with a spectrum analyzer ($f_s = 16.26$ kHz at 600 MeV).

Figure 5 compares the values obtained using the two methods, in the same experiment. These are in good agreement, apart from an absolute difference of 15 ps.

D. Transverse sizes

The transverse sizes of the positron beam are determined by the emittance of the ring, the β functions [14],

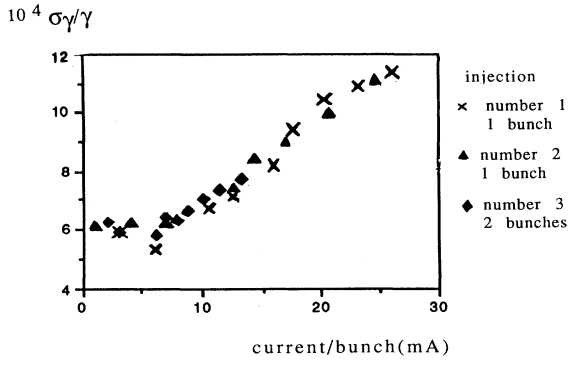

FIG. 4. Energy spread σ_γ/γ vs the ring current per bunch. Electron energy, 600 MeV.

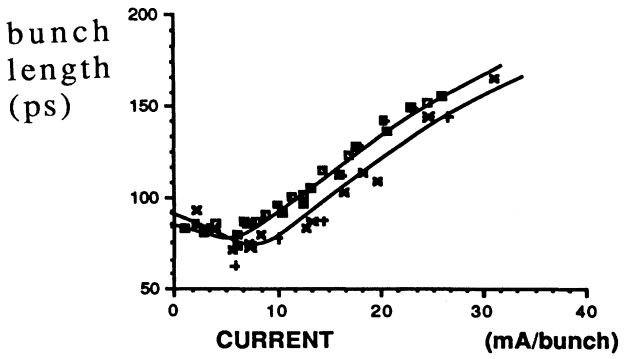

FIG. 5. Comparison of the bunch-length values deduced from a direct time measurement (×) with a pickup station and from the energy spread (□) following Eq. (4).

and the coupling factor between the wave numbers. For the FEL operation, the usual "low emittance" optics of the Super-ACO is used, but with β_z functions reduced by a factor of 2 at the optical klystron location. This operating point is also on a coupling resonance of the Super-ACO, and provides a longer lifetime and a circular-cross-section particle beam which optimizes the filling factor. In both cases, the transverse sizes are

		β_x (m)	β_z (m)	σ_x (μm)	σ_z (μm)
Classical	β_z	5.6	11.2	320	390
Reduced	β_z	5.8	5.7	300	295

From the experimental measurements, taking into account the modifications of the electron density, the filling factor, and the modulation rate, the gain is enhanced by 20% to 30% when the reduced β_z functions are used.

E. Gain at 600-MeV laser oscillation

The optimized gain for the resonant wavelength λ_T can be evaluated from the relationship [6]

$$g = 1.12\times10^{-13}(N+N_d)K^2L_{OK}^2(\mathcal{J})^2 f\rho_e/\gamma^3 ,$$

$$(\mathcal{J})^2 = [J_1(\xi)-J_0(\xi)]^2, \quad \xi = K^2/4+2K^2 . \quad (5)$$

To evaluate the gain, we use the measured values of parameters that were described in the preceding sections. Figure 6 represents the calculated gain for two positron bunches at 600 MeV, for a wavelength of 633 nm and a ring current ranging from 0 to 30 mA per bunch. For a current higher than 8 mA the gain is practically a constant close to 2%, and decreases linearly for lower current.

Under such conditions, the FEL oscillation is currently obtained with two bunches stored in the ring, and for a wide range of current from 2 to 50 mA per bunch, since February 1989. This shows that a gain-over-loss ratio around 4 is obtained. Experimental determination of the actual losses is difficult, as explained in Sec. V. However, the analysis of the laser features indicates that an effective gain of 2% is certainly obtained at high current.

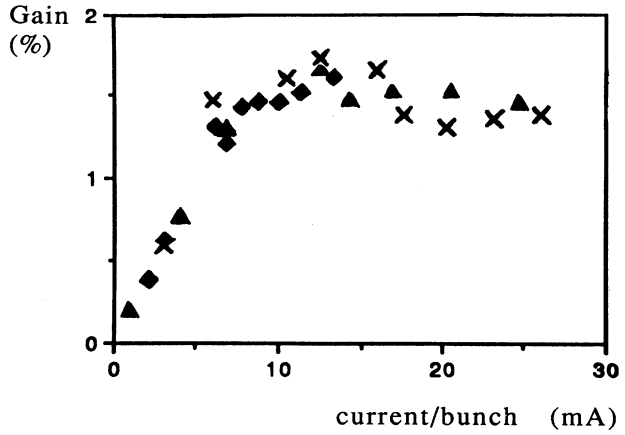

FIG. 6. Calculated gain value vs the ring current per bunch for the Super-ACO at 600 MeV and $\lambda=630$ nm: for one bunch stored during the first injection ($\times$), during the second one (▲), and for two bunches stored during the third injection (♦).

Recently we have also obtained laser oscillation with only one bunch stored in the ring, that is to say, an interaction at each two round trips in the optical cavity.

F. Effect of coherent oscillations on the gain

Theoretical gain estimates assume that the positron bunches are stable, with simple Gaussian shape. In fact, it is well known that in storage rings coherent synchrotron oscillations can develop. As a first approximation those oscillations increase the averaged energy spread. Our estimate of the gain from Eq. (5) takes into account this average value, since we use experimentally determined values of the parameters. However, laser oscillation is extremely sensitive to very small detuning between electrons and photons, and it is not clear whether the dynamical evolution of the electron bunch shape and revolution period at the synchrotron frequency (and its harmonics) affect the gain averaged over a long time.

The Super-ACO FEL operates with synchrotron feedback that is used to stabilize two opposite bunches stored in the ring (dipolar oscillations). Unfortunately the feedback has no effect on multipolar oscillations, and sometimes a drastic reduction in gain is observed as a result of these oscillations. The gain evaluation from Eq. (5) should be considered as a possible maximum value for a perfectly stable positron bunch without dynamic evolution on a short time scale.

IV. FEL OPERATION

For oscillation to result many different parameters must be simultaneously adjusted. The overlap between the photon and positron pulses must be maximized. The cavity length is roughly adjusted and the rf is adjusted for a fine tuning. The dispersive section gap is also optimized and the electron-beam parameters varied (i.e., wave numbers, minimization of the coherent synchrotron oscillation, etc.). The laser oscillation has been obtained in the visible spectrum at 600 MeV, initially, and later at 650 MeV. The laser can now operate over several hours from 50 to 2 mA per bunch. The most sensitive parameter is the cavity length (a detuning around 60 μm stops the laser) and the presence of coherent multipolar synchrotron oscillations can adversely affect operation. In this section we present the general features of the laser, except for the lower power, which will be described in a subsequent section.

A. Spectral characteristics

The laser wavelength is centered around 620 nm, with a wavelength tunability of 500 Å, in good agreement with the mirror bandwidth. The measured spectral width is 1.2 Å with a $\Delta\lambda/\lambda\simeq 2\times 10^{-4}$ (Fig. 7). As in the ACO and the VEPP3, a large broadening of the laser line is obtained, the origin of which is not clear. Spectral narrowing can only be obtained by inserting a dispersive element inside the optical cavity.

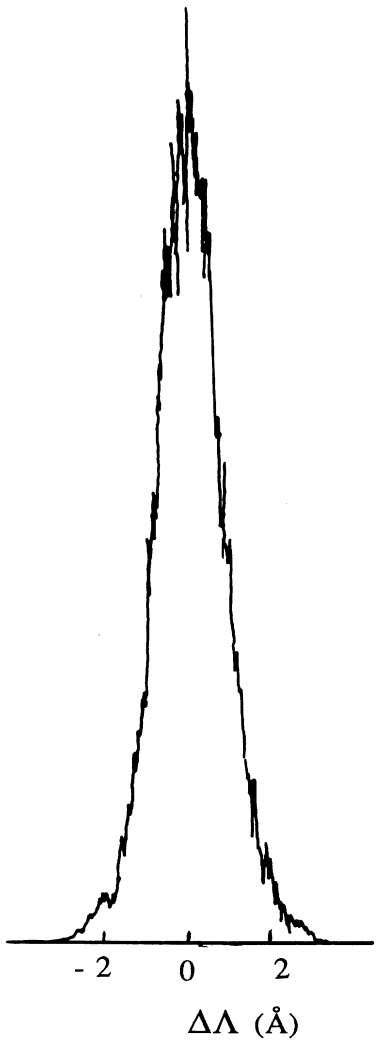

FIG. 7. Typical laser line for the Super-ACO FEL.

B. Temporal structure

Apart from the microtemporal structure due to the revolution of the bunches inside the storage ring, the laser generally adopts a "continuous" structure on a long-time scale. This behavior results from the good stability of the positron bunches. Figure 8 shows the continuous regime generally obtained on the Super-ACO with fluctuations of the order of a few percent. However, during several experiments a pulsed macrotemporal structure appears, as observed on the ACO [10,15] and the VEPP3 [16]. Sometimes the behavior can be clearly attributed to mechanical vibrations of the optical cavity, so that the laser is randomly noisy or pulsed at the line frequency. But generally the natural temporal structure is determined in a complicated way by the electron bunch. This has made it difficult for experimentalists to exactly control the characteristics of the temporal structure.

Figure 9 illustrates start-up phenomena obtained with a Q-switched operation, where the gain is first suppressed by a large rf detuning so as to have the positron bunch in an initial state (with the laser off) and, then, subsequently restored by very rapid rf tuning. The observed temporal structure can be interpreted as follows: the intense first laser pulse begins from a nonmodified positron bunch with maximum gain. The energy spread then increases because of bunch heating and the gain is thus reduced according to its exponential energy spread dependence [Eq. (3)] until a value lower than cavity losses and laser action stops. The energy spread then relaxes with the synchrotron damping time, and when it reaches the loss value, the laser starts again. This is the "saturation" mechanism of SRFEL's. With a stable beam the laser immediately adopts a noisy "continuous" regime, as in Fig. 9. Otherwise, relaxation oscillations appear and the laser exhibits a pulsed structure. The Q-switched operation allows us to increase the peak power, as illustrated in Fig. 9, and it also provides *in situ* measurements of the gain and optical cavity losses [10] from the rise and decay times.

C. Transverse profile of the FEL

Figure 10 shows two photographs of the laser spot shape as viewed on the exit mirror. Without misaligning

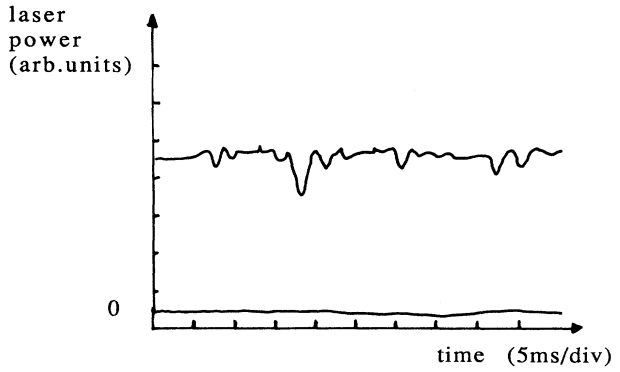

FIG. 8. Macrotemporal structure for a cw FEL obtained when the storage ring is very stable. Time scale, 5 msec/div.

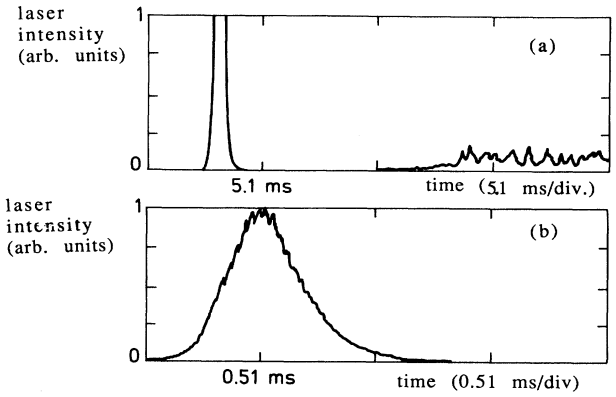

FIG. 9. Q-switch operation. (a) Start-up phenomena after a long rf detuning. The macrotemporal structure exhibits an intense pulse laser after a low evolution towards a cw regime. (b) Expansion of the first laser pulse showing the exponential rise and decay times.

the cavity optical axes and the positron trajectory, the central part of the laser profile generally corresponds to a TEM_{00} mode, as illustrated in Fig. 10(a). This situation is maintained as long as the misalignment does not exceed 0.5 mm, corresponding approximately to the beam waist of the laser. For larger misalignment or a small angle between the optical axis and the trajectory, and also if the

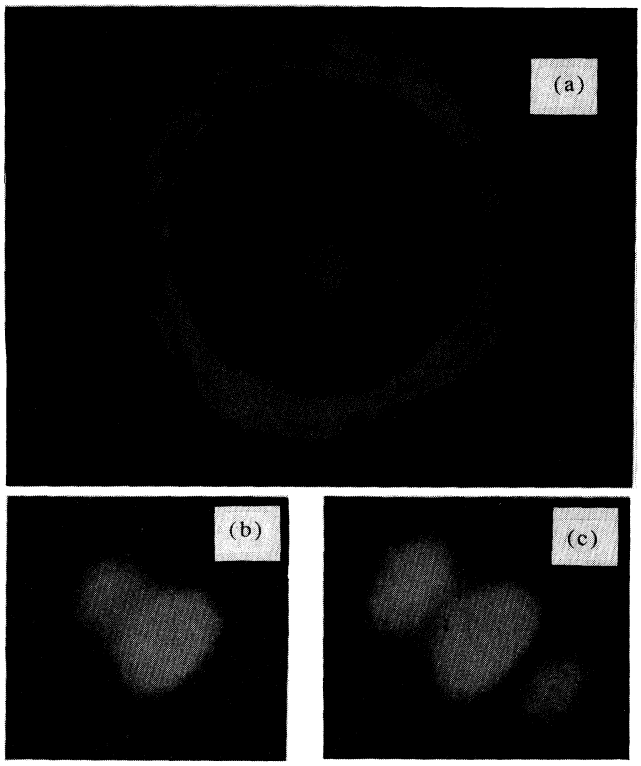

FIG. 10. Photographs of the laser emission as viewed on the exit mirror. (a) The central spot corresponds to a TEM_{00} mode and the aureola corresponds to the uncoated part of the mirror. (b) and (c) Central spot for a TEM_{01} and TEM_{02} operation, respectively.

beam shape is ellipsoidal, the laser oscillates on a practically pure TEM_{01} mode [Fig. 10(b)], or a TEM_{02} mode with its symmetry axis close to the horizontal or vertical plane following the direction of the misalignment. In some cases a superposition of several transverse modes can occur; up to TEM_{05} has been observed. We must note that these modes generally appear as TEM_{0n} only in one direction. In one exceptional case, we have observed a TEM_{11} mode.

These results show that the experiments on the Super-ACO have been performed with a gain-to-loss ratio of the order of 4, as explained in Sec. V, and also that oscillation on the TEM_{00} mode requires the absence of asymmetry in the arrangement optical cavity plus positron beam, such as misalignment, elliptical positron beam section, mechanical vibrations, etc.

The second interesting result concerns the radial extension of the laser power to a distance of several times the beam waist size ($w=2.4$ mm on the mirror). The experiments were performed with mirrors of a diameter of 25 mm, coated only to a diameter of 18 mm. Figure 10(a) shows an aureola corresponding to the laser power transmitted outside the coated part, at a distance of $r \simeq 7w$ or $8w$ in both the x and z directions, with a slightly wider extension in the horizontal plane. The measured laser power extracted through the aureola is around 10 to 20 times the measured power contained in the central TEM_{00} spot. Then, nearly all the power was extracted via a long tail of the radial distribution in a region of mirror transparency. From these power measurements, from the coated and uncoated areas of the mirror and the mirror transmission ($T=8\times10^{-5}$), information can be deduced on the *intracavity* profile and the actual value of the cavity losses.

The intracavity power-density profile is practically a pure TEM_{00} mode (without misalignment) in the central part, with a long tail extending widely beyond this predominant mode. The ratio between the power density in W/cm^2 for the aureola and the peak power density of the central spot can be estimated as

$$P(r \simeq 4.5w) \simeq (5\text{–}8)\times10^{-5} P(r=0) .$$

Such power density cannot be explained with only the low-order mode because the density [$P=\exp(-2r^2/w^2)$] would be given in the range of 10^{-17} for the power at $4.5w$. Radial distribution of the order of 10^{-4} to 10^{-5}, up to $r \simeq 7w$, requires a combination of very-high-order modes ($n>6$ for $r \simeq 4w$ and $n>20$ for $r \simeq 7w$). This point will be clarified in Sec. V.

The second consequence of this long tail concerns the cavity losses, which cannot be evaluated solely from reflectivity measurements. Additional losses arising from the fraction of the power, leaving out the uncoated part of the mirror, depend on the actual laser operation, i.e., the position of the laser distribution with respect to the center of the mirror, the distribution width depending on the adjustment, the mirror reflectivity, etc. From the power measurements performed with mirrors of transmission $T=8\times10^{-5}$, the additional losses per mirror are estimated as $p_a \simeq (2\text{–}3)\times10^{-3}$ for the aureola. The losses due to the coating reflectivity being $p_r \simeq 1\times10^{-3}$ (for undegraded mirrors), the total cavity losses were $p \simeq (6\text{–}8)\times10^{-3}$, the main part being due to the radial extension. Note that losses due to the mirror degradation (see Sec. II) must be added at this value. Moreover, laser operation cannot only be described through a unique value of losses, but must include a transverse profile of losses (on the mirror), or equivalently, a set of loss values p_{nm} for each TEM_{nm} mode.

From these experimental results it can be concluded that the transverse profile of the laser wave has a prominent role in the laser operation (threshold, equilibrium condition, exit power, etc.) Section V will be devoted to a theoretical analysis of transverse effects, to explain the results of the exit power measurements given in this section and Sec. VI.

V. ANALYSIS OF THE TRANSVERSE PROFILE FOR DOMINANT MODES

A complete description of laser operation on a storage ring would require a three-dimensional approach that takes into account the macrotemporal evolution, saturation phenomena, and all possible misalignments between the photon and positron beam. In this section only a few aspects of this general problem are described, to have an idea of the origin of the observed effects and possibly their order of magnitude. The laser wave can be described as a superposition of orthogonal transverse optical modes:

$$E(x,z)=\sum_n a_n \varphi_n(x,z) ,$$

where $\varphi_n(x,z)$ are the eigenmodes of the cavity, well adapted to a description of FEL operation. Then the mirror losses can be represented by a diagonal matrix for the reflectivity [r_{nn}], and the amplifying medium (i.e., the optical klystron) by a general gain matrix [G_{nm}] [17]. These matrices relate the amplitudes of the following eigenmodes:

$$\{a_n\}_{\text{out}}=[M_{nm}]\{a_n\}_{\text{in}} .$$

However, for a resonator having a limited mirror aperture, the eigenmodes cannot be described analytically. Here, to describe $E(x,z)$, we use the set of classical Gaussian modes [18] corresponding to the case of infinite mirror aperture and zero gain, which are convenient for simple calculations. For modes with a radial extension smaller than the width of mirrors ($n<10$ in our case), Gaussian modes are a good approximation of the eigenmodes. For high-order modes, caution must be taken in the physical interpretation of the mathematical calculation, because the eigenmodes are not Gaussian.

A. Symmetry considerations

To describe an optical resonator with a cylindrical symmetry (spherical mirrors with circular section), a set of cylindrical eigenmodes is generally chosen. However, the actual symmetry of the FEL wave depends both on the amplifying medium (the positron beam) and on the

alignment of both optical cavity and positron beam. So, the following elements should be considered.

(a) The positron beam cross section can be ellipsoidal.

(b) The symmetry of the spontaneous emission (which cannot be completely neglected for a low-gain system) is not exactly cylindrical.

(c) A possible misalignment between the optical cavity axis and the mean positron trajectory can define a symmetry plane.

(d) The possible defects and the focusing effects [19] of the optical klystron can affect the mean positron trajectory or the beam cross section.

Generally speaking, these effects destroy all symmetry. Cylindrical symmetry cannot be conserved and, at best, only approximate rectangular symmetry of second order (one symmetry plane) can be considered. Then the good set of eigenmodes is the rectangular TEM_{xz} modes, which have been observed at Orsay and Novosibirsk. Moreover, the approximate second-order symmetry explains why only the TEM_{0n} mode appears as the dominant mode, as shown in Sec. IV.

In this section, calculations have been made only for a unidimensional radial extension, that is to say, TEM_{0n} modes designated here for simplicity as n modes; the electric field at the beam waist is given by [18]

$$E(x)=\sum_n \frac{a_n}{(\sqrt{\pi}2^n n!)^{1/2}} H_n\left[\sqrt{2}\frac{x}{w_0}\right] e^{-x^2/w_0^2}, \quad (6)$$

where H_n is the Hermite polynomial of order n, w_0 the beam waist, and a_n the amplitude of the normalized mode.

B. Gain of a transverse TEM_{0n} mode: The diagonal term of the gain matrix

As a first approximation, neglecting mode mixing (see Sec. V C) and some corrections due to the undulator length [7], the gain is proportional to the filling factor F_f, simply defined as the overlap between the laser intensity profile and the positron beam cross section, in the beam waist plane. For a simple Gaussian positron beam profile,

$$\rho(x)=\rho_M \exp[-(x-x_0)^2/2\sigma_e^2],$$

where x_0 represents a misalignment with respect to the optical axis, the filling factor of an n mode is given by

$$(F_f)_n=\frac{\rho_M}{\sqrt{\pi}2^n n!}\int_{--}^{+-} \exp\left[-\frac{(x-x_0)^2}{2\sigma_e^2}-\frac{2x^2}{w_0^2}\right] \times H_n^2\left[\sqrt{2}\frac{x}{w_0}\right]dx,$$

which can easily be calculated analytically. For convenience, $(F_f)_n$ is normalized with respect to $F_f(n=0, x_0=0)$, leading to the gain reduction with respect to a perfectly centered 0 mode. For a real TEM_{xz} mode the reduction factor is simply expressed as the product of the reduction for both directions.

Figure 11 illustrates the dependence of this reduction

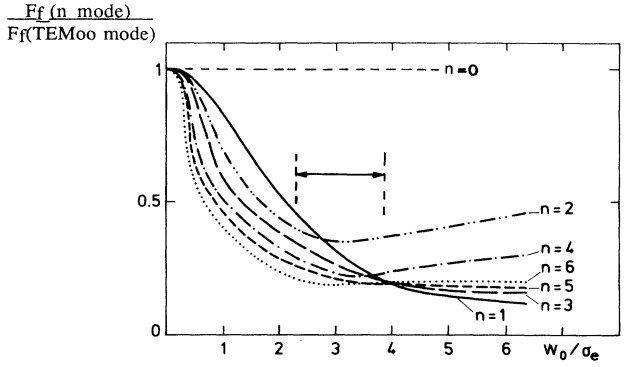

FIG. 11. Reduction of the filling factor (with respect to the TEM_{00} case) vs the ratio of the photon (w_0) and electron (σ_e) beam sizes, for different transverse n modes, the electron beam being perfectly centered on the optical cavity axis. $\leftrightarrow$ indicates the Super-ACO case for $\lambda \simeq 6300$ Å.

factor versus w_0/σ, the ratio between the photon and the positron beam sizes and the mode order n, in the case of a perfectly centered beam $x_0=0$. The Super-ACO optical cavity phase been optimized for the TEM_{00} mode, so that realistic positron beams correspond to a value $2.5<w_0/\sigma<4$. Then the gain reduction falls to a level of 0.25–0.4 for $n=1$, and slowly decreases with the mode order n (reduction factor of 0.2 for $n=6$). Then, even for a perfectly centered beam, substantial gain allows the laser to oscillate simultaneously on several modes, as has been observed experimentally, or at least with a dominant 0 mode and an important amplification of the spontaneous emission for the other modes. In our experiments (see Sec. IV) the gain-over-losses ratio for a 0 mode is estimated as $g/p \simeq 10$ when only low-order modes are present and $g/p \simeq 2$ when taking into account the long tail of the radial distribution. It is therefore not surprising that the threshold is reached simultaneously for several n modes.

Figure 12 illustrates the dependence of the gain versus the off-axis distance x_0 for a realistic positron beam

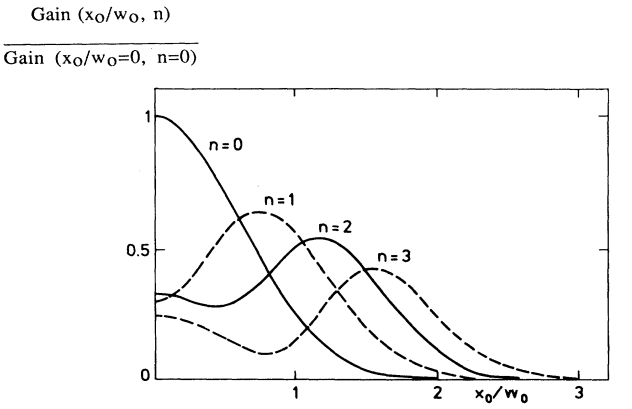

FIG. 12. Reduction of the gain (with respect to the perfectly centered TEM_{00} case) for different transverse modes vs the off-axis position of the electron beam. Horizontal scale: x_0 is the position of the electron beam and w_0 the laser beam waist.

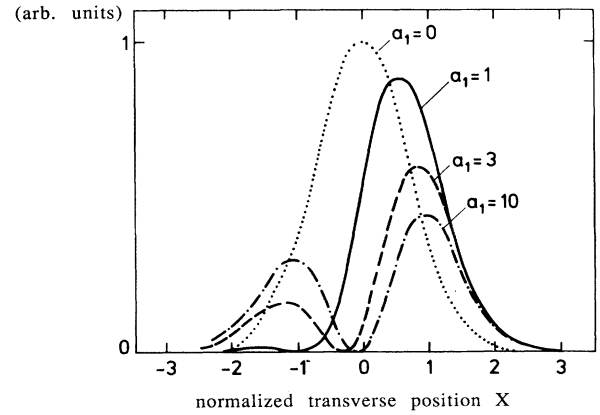

FIG. 13. Theoretical transverse intensity profiles corresponding to a superposition of the electric fields $E=E_0+a_1E_1$ with E_0 and E_1 the electric fields representing, respectively, the TEM_{00} and TEM_{01} modes.

$w_0/\sigma \simeq 3$. As expected, the gain is maximum at a distance x_0 corresponding to the maximum electric field of an n mode where it overcomes the other modes. At these positrons the gain reduction is rather low, so that the threshold is easily reached if $g(n=0)/p > 2$ or 3. Experimentally a simple translation of the electron beam relative to the optical axis induces a jump from $n=0$ to 1 and 2 for distances corresponding to the maximum of Fig. 12.

The question then arises of how does one experimentalist determine the mode components from a transverse profile. The number of zeros (or minima) appearing in the transverse profile simply gives the dominant mode. Difficulties arise when a superposition of several modes of comparable intensities exist. For example, in the case represented in Fig. 10(b), the asymmetry of the lobes indicates that a 1 mode is dominant, though with a nonnegligible 0 mode and perhaps a few other modes. These difficulties are exemplified in the theoretical curves of Fig. 13, where we have represented a combination of 0 and 1 modes *in phase*. It can be seen that for equal intensities the profile is very close to the fundamental mode (except for an experimentally undetectable translation), and the two visible lobes appear only when the 1 mode is largely dominant.

Great case must be taken when analyzing a laser profile, even with an exact recording of $I(x)$. Even for a distribution such as that in Fig. 10(a) a superposition of several modes cannot be excluded; lateral lobes of low intensity are often visible as companions of the central spot.

VI. ANALYSIS OF THE LONG TAIL OF THE TRANSVERSE PROFILE

In the preceding section, dominant modes corresponding to dominant diagonal gain matrix elements have been considered. The explanation of the long tail of the transverse profile requires a more complicated treatment, taking into account the off-diagonal gain matrix elements, that is to say, the mode mixing by the amplifying medium and also the mirror-loss matrix.

A. Gain matrix

Neglecting the effect of the length of the undulator, the electric field transforms at each single pass, through the transverse gain profile $g(X)$, as

$$E_{\text{out}}(X)=[1+g(X)]E_{\text{in}}(X) ,$$

with the input mode expansion $E_{\text{in}}(X)=\sum_n a_n\psi_n(X)$, where $\psi_n(X)$ is the normalized profile of a mode and $X=\sqrt{2}x/w_0$. The amplified part $g(X)E_{\text{in}}(X)$ corresponds to another mode expansion: $g(X)E_{\text{in}}(X)=\sum_n d_n\psi_n(X)$, with $d_n=\sum_k g_{nk}a_k$, so that the mode mixing due to the undulator is defined by the gain matrix:

$$g_{nk}=\frac{1}{(\pi 2^n n!2^k k!)^{1/2}}\int_{-\infty}^{+\infty} g(X)e^{-X^2}H_n(X)H_k(X)dX . \tag{7}$$

The gain matrix then appears as a generalized filling factor, i.e., the overlap between $g(X)$ and the cross term for two modes. For convenience the gain matrix will be normalized with respect to g_{00}, so that the g_{nk} elements represent the gain reduction compared to an ideal case of a single 0 mode perfectly centered. In this paper we consider mainly the case of a unidimensional model. For a real TEM_{xz} mode the gain elements are products, $g_{nk}(x)$, $g_{n'k'}(z)$ depending of four indices.

Table V presents the gain matrix corresponding to the Super-ACO experiment for the case of a centered gain profile:

$$g(x)=g_0\exp(-x^2/2\sigma^2) \quad \text{with } w_0/\sigma_e=3.5 .$$

It is clear that the higher-order elements cannot be neglected (see, for example, $g_{20,4}$ or $g_{30,20}$ in Table V), and efficient mode mixing can appear among a great number of modes.

However, considering only the gain matrix is not sufficient to describe the laser mode structure: an explicit calculation of the amplitudes a_n at equilibrium, after one round trip inside the optical cavity, is necessary. Simulations with bidimensional TEM modes and a real positron beam shape can only be carried out numerically, requiring a large number of calculations, because a gain matrix of around 400×400 must be considered. These calculations are not really worth performing, as additional experimental defects of a realistic experiment are neglected, e.g., real beam shape, off-axis effects, etc.

However, the order of magnitude of the mode mixing effects can be estimated using a simple model that neglects the width σ_e. A simple analytical solution for the laser profile can be found. By replacing the gain profile by $g(X)=g_0\delta(X_0)$ the matrix elements (7) are simple products:

$$g_{nk}=g_0e^{-X_0^2}g_ng_k, \quad \text{where } g_n=\frac{H_n(X_0)}{(\sqrt{n}\,2^n n!)^{1/2}} . \tag{8}$$

Table VI gives the gain matrix for a centered beam $X_0=0$. Comparing with the real case of Table V, two main differences are evident: (i) the elements far from the diagonal are larger, leading to more efficient mode mixing

TABLE V. Gain matrix G_{nk} for Super-ACO with a perfectly centered electron beam of width $\sigma_e = 0.3 w_0$. The matrix is symmetric; only the upper part is presented.

	0	1	2	3	4	19	20	29	30
0	1.00	0	0.57	0	0.39	0	0.05	0	−0.01
1		0.20	0	−0.20	0	−0.05	0	0.02	0
2			0.36	0	−0.28	0	−0.06	0	0.02
3				0.20	0	0.07	0	−0.03	0
4					0.23	0	0.07	0	0.03
19						−0.08	0	−0.08	0
20							−0.08	0	−0.08
29								0.08	0
30									0.08

and (ii) the odd modes disappear, leading to less efficient mode mixing. Numerical calculations using (7) show that the model is a good approximation for $\sigma_e / w_0 < 0.15$. For the experiments on the Super-ACO, $\sigma_e / w_0 \simeq 0.3$.

The effect of an off-axis position is illustrated in Table VII showing the matrix for $X_0 = 1.58$ corresponding to the main maximum of the TEM_{02} field. The gain reduction is small ($g_{22} = 0.66$), and important mode mixing appears between odd and even modes.

B. Equilibrium condition

At equilibrium, the laser is continuous without any macrotemporal structure. Designating the electric field of a micropulse as $E(x,z,t)$ (duration lower than 0.1 ns), this field can be represented as a Fourier transform,

$$E(x,z,t) = \sum_{n,m} \psi_{nm}(x,z) \int A_{nm}(\omega) e^{i[\omega t + \varphi_{nm}(\omega)]} d\omega \ ,$$

where φ_{nm} is the normalized profile of a TEM_{nm} mode; A_{nm} and φ_{nm} together define the complex field amplitude for each transverse mode.

After one round trip in the optical cavity (transit time 120 ns) the equilibrium condition requires the reproductibility of the micropulse in both the transverse and the temporal dimensions, that is to say, *the reproductibility of the complex amplitude* $A_{nm} e^{i\varphi nm}$ *for each spectral component of each transverse mode.*

After one round trip the new wave vector for each spectral component is given by

$$(I + G)(r^2 e^{i\Phi})\{a_n\} + \{s_n\} \ .$$

The vector $\{a_n\}$ represents the electric field at the exit of the undulator (each mode is designated here by a simple index subscript n), I is the identity matrix, G the gain matrix, the matrix $r^2 e^{i\phi}$ describes the propagation of the wave and the mirror reflectivities, and the vector $\{s_n\}$ represents the spontaneous emission in terms of transverse modes. The equilibrium leads to a general set of equations:

$$[I - (I + G)(r^2 e^{i\Phi})]\{a_n\} = \{s_n\} \ , \tag{9}$$

which can only be solved numerically in general and also requires knowledge of the spontaneous-emission distribution. Here we neglect mode mixing due to the limited aperture of mirrors and assume that the main effect of the mirror's reflectivity can be described by a simple diagonal matrix giving the diffraction losses for each mode (this hypothesis is completely valid when the ψ_{nm} functions are eigenmodes of the optical cavity).

Let us first consider the case $\sigma_e \gg w_0$. The gain profile is constant, $g(x) = g_0$, and from Eq. (7), G is diagonal with $g_{nn} = g_0$ and

TABLE VI. Gain matrix G_{nk} for the limit model $g(x) = G_0 \delta(0)$.

	0	2	4	6	8	20	30
0	1.00	−0.71	0.61	−0.56	0.52	0.42	−0.38
2		0.50	−0.43	0.40	−0.37	−0.30	0.27
4			0.38	−0.34	0.32	0.26	−0.23
6				0.31	−0.29	−0.23	0.21
8					0.27	0.22	−0.20
20						0.18	−0.16
30							0.12

TABLE VII. Gain matrix for the limit model for an off-axis beam corresponding to the main maxima of TEM_{02}.

	0	1	2	3	4	10
0	0.08	0.18	0.23	0.15	−0.03	−0.10
1		0.41	0.52	0.34	−0.07	−0.22
2			0.66	0.42	−0.09	−0.28
3				0.27	−0.06	−0.18
4					0.01	0.04
10						0.12

$$a_n = \frac{s_n}{1-(1+g_0)r_n^2 e^{i\Phi_n}} . \quad (10)$$

There is no mode mixing and the amplitudes are governed by the phase change after one round trip:

$$\Phi_{nm} = \frac{4\pi d}{\lambda} - 4(m+n+1)\arctan[d/(2R_c-d)]^{-1/2} . \quad (11)$$

Significant amplitudes can only develop for resonant wavelengths corresponding to $\Phi_{mn}=2p\pi$. The electric-field profile is therefore that of the spontaneous emission modified by the spectral response of the optical cavity.

However, in general, $\sigma_e < w_0$, and the gain matrix is not diagonal. As a first approximation, we choose the limit $g(x)=g_0\delta(r_0)$ and neglect the spontaneous emission. Equation (10) can therefore be rewritten as

$$(1-r_n^2 e^{i\Phi_n})a_n = g_n \sum_{k=0}^{\infty} g_k r_k^2 e^{i\Phi_k} a_k ,$$

giving the ratio of the intensity I_n with respect to a dominant mode i_D as

$$\frac{I_n}{I_D} = \left[\frac{a_n}{a_D}\right]^2 = \left[\frac{g_n}{g_D}\right]^2 \frac{(1+r_D^4-2r_D^2\cos\Phi_D)}{(1+r_n^4-2r_n^2\cos\Phi_n)} , \quad (12)$$

and therefore the eigenmodes of the laser.

For wavelengths where the dominant mode is resonant, significant intensities can only be realized for other modes that are close to the resonance $\Phi_n=2p\pi$. From Eq. (11), it can be seen that such a condition is generally not satisfied and the intensity is close to the minimum value:

$$\frac{I_n}{I_D} = \left[\frac{g_n}{g_D}\right]^2 \left[\frac{1-r_D^2}{1+r_n^2}\right]^2 ,$$

which is very low. However, g_n slowly decreases with the order mode so that a great number of modes have comparable intensities.

Table VIII gives the result of a one-dimensional calculation (modes TEM_{0n} only) for the Super-ACO with different mirror reflectivities and dominant modes in the case of a perfectly centered beam. I_n fluctuates by several orders of magnitude and is very dependent on the mirror reflectivity and the order of dominant mode. These calculations are summarized by an average value $\langle I_n \rangle$ per mode for the modes other than the dominant one, which can be used to estimate the total intensity in the real case. From our experiments, performed with $r^2 \simeq 0.995$, around 40 one-dimensional modes must be considered, so that from Table VIII the total intensity is of the order of 10^{-3}, slowly depending on the dominant mode. This is consistent with our experimental estimate (Sec. IV C).

C. General conclusions for the laser transverse profile

The above calculations have been made using a simple one-dimensional limit model leading to some general conclusions that are valid for a more realistic laser profile.

(a) The eigenmode of the laser is no longer Gaussian and has a large radial extension. This has consequences on the exit laser power and the estimation of the optical cavity losses, which will be detailed in Sec. VII.

(b) For mirrors of reasonable aperture, the eigenmode is mainly determined by the gain profile. A limited mirror aperture has no important effect, as illustrated by the values of $\langle I_n \rangle$ per mode of Table VIII, except when the aperture becomes of the order of the central "spot" or perhaps when the mirrors are highly transparent.

(c) The experimental analysis of the laser profile becomes very difficult since an eigenmode can eventually have secondary maxima, a situation which cannot easily be distinguished from a superposition from several eigenmodes due, for example, to different resonant wavelengths [Eq. (11) with $\Phi_{nm}=2p\pi$]. Actually, for large spectral laser linewidth, the analysis of a transverse profile probably cannot be performed without considering the partition of the longitudinal modes.

(d) For an off-axis electron beam, even and odd modes can appear with important coupling between them. Generally asymmetric profiles will be obtained as illustrated in Fig. 10(b).

(e) Realistic two-dimensional (2D) models lead to an area extension of the "long tail," even for a TEM_{0n} dominant mode. For a given wavelength all x-z modes with the same $m+n$ value are in phase [Eq. (11)], and are highly coupled together, giving a large area extension in all x-z directions. Experimentally such an extension is observed whatever the dominant mode might be.

Particular transverse profiles can appear for particular values of the mirror curvature. If $\Phi_{mn}=2p\pi$ the corre-

TABLE VIII. I_n values [Eq. (12)] for different dominant modes and different mirror reflectivities.

Dominant mode / r^2 / n	TEM_{00}		TEM_{02}		TEM_{04}	
	0.995	0.98	0.995	0.98	0.995	0.98
0	1	1	13.6×10^{-6}		58×10^{-6}	
2	3.4×10^{-6}	55×10^{-6}	1		9	
4	8.1×10^{-6}	130×10^{-6}	5.1×10^{-6}		1	
6	4.5×10^{-6}	73×10^{-6}	13.6×10^{-6}		5.7×10^{-6}	
8	2.1×10^{-6}	34×10^{-6}	7.9×10^{-6}		16×10^{-6}	
10	68×10^{-6}	1090×10^{-6}	3.8×10^{-6}		9.5×10^{-6}	
30	4.7×10^{-6}	76×10^{-6}	3×10^{-6}		3.3×10^{-6}	
32	0.9×10^{-6}	15×10^{-6}	9×10^{-6}		4.3×10^{-6}	
34	68×10^{-6}	1098×10^{-6}	1.7×10^{-6}		11.7×10^{-6}	
36	1×10^{-6}	16×10^{-6}	132×10^{-6}		2.2×10^{-6}	
	$\langle I_n\rangle$ per mode					
	1×10^{-5}	17×10^{-5}	2×10^{-5}	32×10^{-5}	2.8×10^{-5}	45×10^{-5}
	$\langle I_n\rangle$ per mode for a calculation with $r_n^2=0$ if $n>20$					
	0.8×10^{-5}	12×10^{-5}				

sponding modes have an intensity nearly equal to that of the dominant mode. For a dominant 0 mode, for example, such a situation occurs when $\sqrt{d/(2R_c-d)}=\tan[p\pi/2(m+n)]$. This gives for the Super-ACO

$m+n$	R_c	Possible (m,n)
4	$10.55m$	(0,4),(2,2),(4,0)
5	9.95	(5,0),(3,2),(2,3),(0,5)
6	9.65	(6,0),(4,2),. . . ,(0,6)
. . .	. . .	
18	10.19 or $9.65m$	(18,0),(16,2),. . . ,(2,16),(0,18)

Some values R_c are close to $R_c=10m$ so that laser profiles with high-order modes can eventually be induced by a small mirror curvature modification (mirror heating, mechanical strains, etc.). Experimentally it seems very difficult to avoid these resonances for high-order Gaussian modes.

(f) The gain model leads to a transverse profile that is practically independent of the absolute value of the gain [Eq. (12)], as long as $\sigma_e<0.19w_0$ and the mirror aperture is larger than the central part of the oscillation eigenmode. So, as a rough conclusion, the transverse profile is relatively unaffected by the absolute gain value, the saturation mechanism and also the spectral width of the laser line relative to the longitudinal mode separation.

These general considerations have consequences on the laser operation and the best choice of parameters for optimizing the laser power, as briefly explained in Sec. VII.

VII. LASER POWER

As explained in Sec. IV C, the laser power is extracted through two different parts of the total area of the mirrors: the central part of the spot is classically extracted with a very low mirror transmissivity $T=7.7\times10^{-5}$, but the most important part of the power is extracted outside the coated part of the mirror, i.e., with a transmissivity $T=1$, corresponding to the area outside the $R=4w$.

Figure 14 shows the laser power versus the ring current obtained with the Super-ACO operating at 600 and 650 MeV, for different experiments. Taking into account the imperfect optimization and some variation of the positron-beam characteristics, the laser power is roughly proportional to the ring current with fluctuations of 50%. No significant differences appear for the experiments where $TEM_{00,\ 01,\ or\ 02}$ modes have been observed or for a 600- or 650-MeV electron energy. Figure 14 also reports the estimated total extracted power, taking into

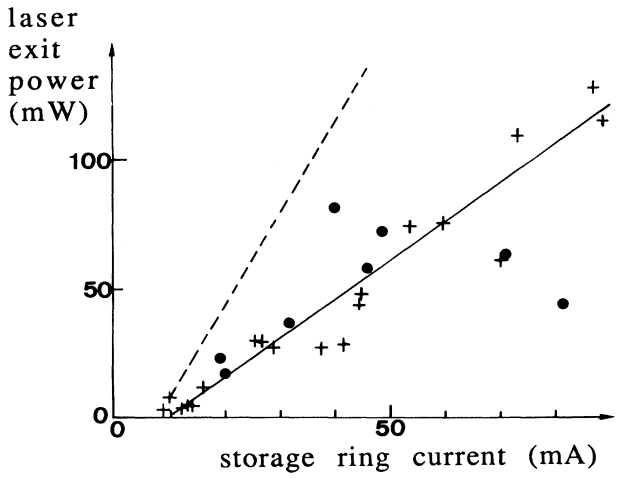

FIG. 14. Measured laser exit power (both mirrors) with respect to the storage-ring current for different experiments: +, 600 MeV; △, 650 MeV; — — —, estimation of the total extracted power including mirror absorption.

account the mirror absorption losses. This latter part has been estimated from the ratio between the mirror transmission and the total mirror losses, measured before and after the series of experiments and corrected for the temporal evolution of the mirror degradation. The total extracted power is 290 mW for a 110-mW measured exit power (both mirrors) and a ring current $i=89$ mA. The corresponding intracavity average power is therefore around 30 to 40 W, and for Q-switched operation at a rate of 10 Hz the theoretical intracavity peak power of a micropulse would be of the order of 30 MW. However, at present there are experimental difficulties arising from the response of the rf cavity to a very rapid frequency change, so that the macropulse rise time is longer than the theoretical one. The exact micropulse width (less than 200 ps) is also unknown so that for the present experimental conditions; the intracavity peak power can be only estimated to be higher than 5 MW.

Table IX illustrates the main characteristics of the laser under different experimental conditions. The main part of the cavity loss is actually due to mirror absorption (which increases with the successive irradiations), and therefore the output power represents only 20–50 % of the total extracted power. Also, because of the transverse profile, only 2–3 % of the total power is transmitted through the coated area of the mirror and 20–50 % via the aureola (no coating).

Table IX also gives the theoretical laser power (Renieri limit) estimated for a perfectly optimized klystron:

$$P=2e^{-1/2}f_0(\sigma_\gamma/\gamma)_0(\sqrt{g_0/p}-\sqrt{p/g_0})P_s\ , \qquad (13)$$

where f_0 is the residual optical modulation rate due to the angular spread ($f_0\simeq 0.98$), $(\sigma_\gamma/\gamma)_0$ is the energy spread without laser (see Fig. 4), g_0 is the initial gain of the system (see Fig. 6), and p are the optical cavity losses (taking into account the reflectivity losses *and* the transmission losses through the uncoated part of the mirror). There is a good agreement between experimental results and theoretical estimations since generally 60% of the possible maximum power is really extracted.

Several questions arise from the eigenmode profile.

(a) The laser power contained in the aureola does not participate in the amplification process and therefore must be considered as a loss equivalent to an additional transmission. In other words, for a FEL, the cavity losses $\mathcal{L}$ cannot be estimated using the classical mirror losses for Gaussian beams, but only with an empirical formula:

$$p=\mathcal{L}_{\text{transmission}}+\mathcal{L}_{\text{absorption}}+\mathcal{L}_{\text{aureola}}\ . \qquad (14)$$

The last term actually corresponds to the diffraction losses of the laser eigenmode, is very difficult to estimate theoretically, and depends very much on the experimental situation. Only experimental determination of the geometry of the exit power gives reliable results.

(b) The best choice of the aperture and transmission of the mirror in order to optimize the gain or the exit power is not clearly evident, because the eigenmode profile depends on these parameters. The first solution gives an enhancement of the transmission. This leaves the transverse profile practically unmodified, with an important fraction of the power transmitted by the uncoated part. For example, with $T=0.5\%$ one expects around 1.3% of total losses with the partitioning: transmission=40%, aureola=20%, and absorption 40%. Otherwise, one could use mirrors of a large coated area like that in the VEPP3 experiment in order to avoid the direct annular transmission. However, calculations as in those presented in Sec. IV shows that a large radial extension will also be obtained; and, in fact, because of the limited gain profile, the long tail does not participate in the amplification process and therefore may be considered as a supplementary loss (in Gaussian terms these high-order modes circulate inside the cavity and are finally absorbed or transmitted by the mirrors without amplification). Because the transverse profile is largely dominated by the gain profile, leaving the dominant Gaussian-mode TEM_{00} practically unchanged, independent of the mirror diameter, perhaps the best solution for the maximization of the exit power is to extract the unamplified high-order Gaussian modes [an annular laser as in Fig. 10(a)] leading to an intracavity TEM_{00} mode suitable for amplification.

TABLE IX. Laser power and cavity losses for several experiments on the Super-ACO.

Ring current (mA)	Cavity losses (%)				Extracted power					Conditions	
	Mirror transmission	Absorption	Aureola	Total losses	Transmitted through the coated area (% of total power)	Transmitted through the aureola (% of total power)	Absorption (% of total power)	Total extracted power (mW)	Theoretical extracted power (mW)		
12	0.021	0.39	0.40	0.81	2.6	48	50	11	20	First set of mirrors	TEM_{00}
27	0.020	0.41	0.25	0.68	3	37	60	78	97		TEM_{01}
71	0.020	0.48	0.28	0.79	2.5	36	61	150	387		TEM_{00}
89	0.020	0.55	0.34	0.92	2.1	37	61	290	478	Second set of mirrors 600 MeV	TEM_{00}
82	0.020	0.64	0.15	0.80	2.5	18	79	236	492		TEM_{00}
71	0.020	0.64	0.20	0.85	2.3	23	75	268	356	650 MeV	TEM_{00}

VIII. CONCLUSION

The Super-ACO free-electron laser is a good device to understand more completely the physics of the storage ring FEL (dynamics, transverse-mode behavior, laser temporal structure, etc.). Some differences are put in evidence, in comparison with the previous results from the ACO and the VEPP3 experiments. Some developments are under study or planned on this system: the chaotic macrotemporal structure [20], deduced from experimental results and theoretical analysis, the study of the microtemporal structure with a fast detector, and some usual laser techniques applied to this FEL in order to improve its characteristics.

ACKNOWLEDGMENTS

This work was supported by Laboratoire pour l'Utilisation du Rayonnement Electromagnétique (LURE), the Centre National de la Recherche Scientifique (CNRS), the Commissariat à l'Energie Atomique (CEN), and the Direction des Recherches et Etudes Techniques (DRET) (Contract No. 85/179). We would like to thank the machine group and the operators of Super-ACO for their help and discussions.

[1] M. Billardon, P. Elleaume, J. M. Ortéga, C. Bazin, M. Bergher, M. Velghe, Y. Petroff, D. A. Deacon, K. E. Robinson, and J. M. J. Madey, Phys. Rev. Lett. **51**, 1652 (1983).

[2] N. A. Vinokurov and V. Litvinienko, in Proceedings of the SR88 Conference, Novosibirsk, 1988 [NIMA **282**, 424 (1989)].

[3] M. E. Couprie, C. Bazin, M. Billardon, and M. Velghe, in *Electron Laser II (1989),* Proceedings of the International Congress on Optical Science and Engineering, Paris, 1989 (International Society for Optical Engineering, Bellingham, WA, 1989), Vol. 1133, p. 2.

[4] M. E. Couprie, thèse de doctorat, Université de Paris–Sud, 1989.

[5] J. C. Besson, P. Certain, A. Daël, P. Juan, A. Labèque, M. P. Level, P. C. Marin, C. Monet-Desombey, P. Nghiem, M. Sommer, R. Souchet, and H. Zyngier, LURE Report No. ANNEAUX/RT/88-01, 1988 (unpublished).

[6] M. E. Couprie, C. Bazin, and M. Billardon, *Magnetic Optimization of the Optical Klystron DOMINO for the Super-ACO Storage Ring Free-Electron Laser (NIMA 278)* (North-Holland, Amsterdam, 1989).

[7] W. B. Colson and P. Elleaume, Appl. Phys. B **29**, 101 (1982).

[8] P. Elleaume, M. Velghe, M. Billardon, and J. M. Ortéga, Appl. Opt. **24**, 2762 (1985).

[9] M. E. Couprie, M. Billardon, M. Velghe, C. Bazin, M. Bergher, H. Fang, J. M. Ortéga, Y. Petroff, and R. Prazeres, Nucl. Instrum. Methods A **272**, 166 (1988).

[10] M. Billardon, P. Elleaume, J. M. Ortéga, C. Bazin, M. Bergher, M. Velghe, D. A. G. Deacon, and Y. Petroff, IEEE J. Quantum Electron. **QE-21**, 805 (1985).

[11] M. Billardon, P. Elleaume, J. M. Ortéga, C. Bazin, M. Bergher, M. E. Couprie, R. Prazeres, M. Velghe, and Y. Petroff, Europhys. Lett. **3**, 689 (1987).

[12] V. Litvinienko, in Proceedings of the 11th International Conference on FEL, Naples, FL, 1989 [NIMA **296**, 1 (1990)].

[13] P. Elleaume, J. Phys. (Paris) Colloq. **44**, C1-353 (1983).

[14] M. Sands, Stanford Linear Accelerator Center Report No. 121, 1970 (unpublished); also in *The Physics of Electron Storage Rings. An Introduction,* Proceedings of the International School of Physics, "Enrico Fermi," Course XXXXVI, 1971, edited by B. Touschek (Academic, New York, 1971), pp. 257–411.

[15] P. Elleaume, J. Phys. (Paris) **45**, 997 (1984).

[16] N. A. Vinokurov, in Proceedings of the SRI-88 Conference, Tsukuba, 1988 [Rev. Sci. Instrum. **60**, 1435 (1989)].

[17] P. Elleaume and D. A. G. Deacon, Appl. Phys. B **33**, 9 (1984).

[18] H. Kogelnik and T. Li, Appl. Opt. **5**, 1550 (1966).

[19] M. Sommer, Super-ACO Report No. 86-29 (unpublished).

[20] M. Billardon, Phys. Rev. Lett. **65**, 713 (1990).

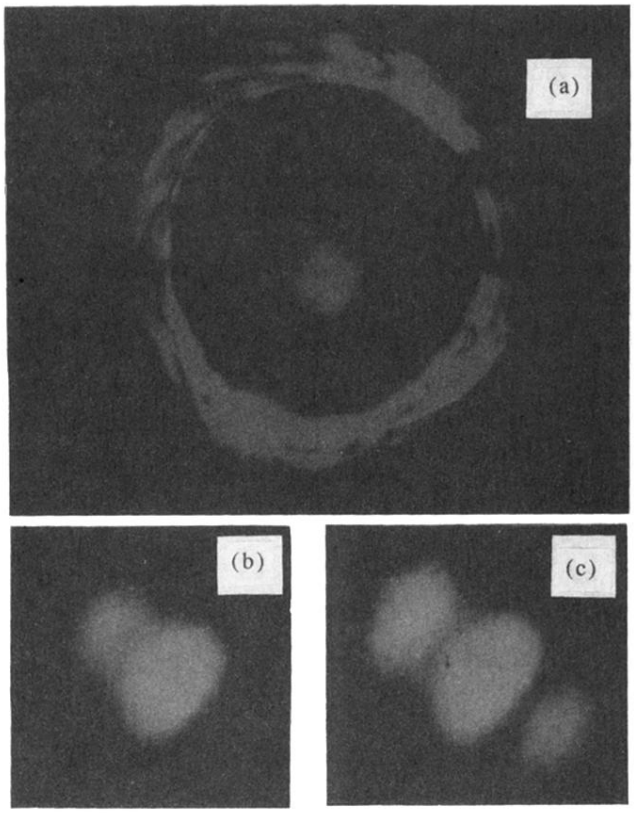

FIG. 10. Photographs of the laser emission as viewed on the exit mirror. (a) The central spot corresponds to a TEM_{00} mode and the aureola corresponds to the uncoated part of the mirror. (b) and (c) Central spot for a TEM_{01} and TEM_{02} operation, respectively.